Avoiding the Deconvolution: Framework Oriented Color Transfer for Enhancing Low-Light Images

Laura Florea[1], Corneliu Florea[1,2] and Ciprian Ionaşcu[1]

[1]Image Processing and Analysis Laboratory, University Politehnica of Bucharest,

[2] Fotonation

{laura.florea; corneliu.florea; cipiran.ionascu}@upb.ro

Abstract

In this paper we introduce a novel color transfer method to address the underexposed image amplification problem. Targeted scenario implies a dual acquisition, containing a normally exposed, possibly blurred, image and an underexposed/low-light but sharp one. The problem of enhancing the low-light image is addressed as a color transfer problem. To properly solve the color transfer, the scene is split into perceptual frameworks and we propose a novel piece-wise approximation. The proposed method is shown to lead to robust results from both an objective and a subjective point of view.

1. Introduction

Digital still camera miniaturization deemed by the huge advances of mobile phones lead to design changes such as optic size diminishing or photo-sensible area shrinking. The small photo-sensible area, indirectly leads to reduced correlation between the incident light and the reported image intensity, thus forcing increased exposure time. Furthermore, since the small photo-sensible area decreases the picture angle and since the human hand jitter is always present, the resulting large exposure time increases the chances that the relative hand tremor induces motion blur. This phenomenon degrades the visual quality of images so that photographers and camera manufactures are frequently searching for methods to limit its effects.

The problem of image degradation due to motion blur is known and, typically, the preferred solution is to estimate the degradation kernel (known as Point Spread Function - PSF) and compensate it. Estimation may be directly from the degraded image and the whole solution is called blind deconvolution (and we kindly ask the reader to refer to the works of Levin et al. [13] and Koutera and Sroubek [11] for reviews on the topic) or by estimation of movement followed by deconvolution (as in the work of Joshi et al. [9]).

The main disadvantage is that, usually, such methods assume the PSF to be spatially invariant (or uniform). Yet, this assumption, according to the measurements reported by Singhy and Riviere [23], is not realistic. Human tremor contains significant components on the Z axis and translational components (that lead to different trajectories for pixels corresponding to different depths [9]) leading to heavily nonstationary PSFs. Notable exceptions that use non-stationary PSF models are the works of Whyte et al. [27] or Sun et al. [24]; however, in both cases the non-uniformity assumed fails to realistically model the natural variation of the human tremor.

Alternatively, one may avoid the circumstances that generate the unwanted motion blur by reducing the exposure time below the "motion limit", which typically is based on the "q over f35" rule [28]. In the here proposed work this strategy is assume .

Furthermore, inspired by the previous works of Drimbarean et al. [2] and of Yuan et al. [29], we acquire two input images: one is normally exposed but possibly blurred and one is underexposed but still. We treat the problem of enhancing the underexposed image as a process of transferring color from the normally exposed image (that in the remainder of the paper will be named the reference image) to the underexposed one (also named subject image).

The main contribution of the proposed paper is the introduction of a perceptually inspired color transfer method adapted to the following dual-image input scenario: (1) the underexposed image is sharp, but it may lack good colors; (2) the normally exposed image may be blurred (from hand motion), but has good colors; (3) the two images contain *almost* the same scene. A secondary contribution of the current work is a theoretical discussion of why underexposing and amplification is a more practical solution than deconvolution.

Thus, the remainder of the paper is organized as follows: in section 2 we will review the prior related work on the topic of color transfer and, respectively, on low-light image enhancement. In section 3 we argue why deconvolution

is not practical and other alternatives should be envisaged. In section 4 we describe the proposed algorithm, while in the subsequent one we present implementation details and achieved results. The paper ends with discussion and conclusions.

2. Related Work

Taking into account that the main contribution is a color transfer method that is used for enhancing low-light images, these topics will be briefly surveyed.

Color transfer (mapping) algorithms aim to recolor a subject image by computing a transfer function (mapping) between that image and another, reference image. Following the recent review on the topic by Faridul et al. [4], color transfer methods may be divided on point-based or region based. In the point based category one should note the very influential work of Reinhard et al. [21] which match the first two statistical moments of the two images in the $l\alpha\beta$ uncorrelated color space introduced earlier, [22]. Yet the work while being simple and intuitive is general and many further enhancement have been proposed to address various scenarios. Also in this category fall the methods proposed by Pitie et al. [19] which maps the N-dimensional color distribution of the reference image onto subject image, or the one introduced by Pouli and Reinhard [20] which performs the mapping pixel-wise but do stage it sequentially by considering pyramidal resolutions. These solutions lead to qualitative results but we consider that they are general transformations which do not adapt well to certain situations such as the one described here.

In the category of region based methods it falls the region consistent method [10]; yet its application is restricted by the assumption that region pairs preserve their monotonicity in the two images, which may not be necessarily fulfilled in our scenario due to different acquisition time. Also, here, Olivera et al. coarsely register two images, segment images into regions (by Expectation-Maximization [17] or mean-shift [18]) and perform transfer from one to the other based on region impairment; conceptually we differ by the fact that we do not assume any registration step thus, we do not encode spatial correspondences between the two images but only color intensities correspondences. Furthermore, we introduce a general mathematical model out of which, given a probabilistic approach and specific choices, these previously proposed methods may be retrieved.

Low-light image enhancement is another area that captured a lot of interest. Recently Fotiadou et al. [5] proposed to enhance low-light image by constructing day and respectively night dictionaries based on sparse representations. Lore et al. [15] showed that low-light enhancement is achievable by the same auto-encoder based deep-net topology that was previously shown to perform denoising. However all methods are based on single image enhancement

and it is reasonable to assume that a reference image should improve the resulting image quality.

3. Hand Tremor and Deconvolution

The motion blur during still image acquisition is due to the involuntary hand tremor. To give an intuition of the probable size of a motion blur kernel (PSF), we will start by reviewing some facts regarding the hand tremor. First let us note that hand tremor was substantially studied in the bioengineering domain as it interferes with microsurgeons ability to keep hands still. Veluvolu and Ang [25] performed a comparative study of microsurgeons and normal people and found that amplitude of movement for microsurgeons is at half of the normal people. Next, using inertial sensors, Singhy and Riviere [23] measured the absolute deviation of the human tremor in microsurgeons and found comparable amplitudes for all three axes. In other words the amplitude of rotational components that generate a certain size of motion blur during an acquisition also exists on the Z axis contributing to the deep non-stationarity of the PSF. Assuming that the spatially variable PSF is completely retrieved (which was not yet achieved in related work), typically [24], the non-stationary deconvolution is highly computationally intensive. For instance Gupta et al. [7] report one hour on CPU to solve 1Mpixel image while Hirsch et al. [8] report 440 secs with GPU acceleration for the same image size.

In parallel, taking into account that Singhy and Riviere [23] report an average displacement for the hand tremor of 22 μm, Veluvolu and Ang [25] a dominant frequency of 4Hz, and high end smartphone camera has a pixel size of 1.12 μm for an exposure of 1/4 sec = 4Hz, a PSF size of 19 pixels may be produced. Also for the same exposure the PSF may be completely non-uniform across the image: the PSF in top left corner may get to be near-perpendicular from the one in bottom right corner.

This paper argues that it is computationally more efficient and the results are more robust if, instead of deconvolution, an underexposing followed by a color transfer oriented method for compensation of the low light is used. The results that will be later presented, show that up to 2 exposure stops may be compensated such way.

4. Framework Oriented Color Transfer

The first notable color transfer method was proposed by Reinhard et al. [21]. In this method, the tones, u, from the source image, I_s, are adjusted, on each chosen color plane independently, according to:

$$g(u) = au + b \qquad (1)$$

The specificity of this mapping is given by the choice of the color planes (taken as uncorrelated planes) and of the constants a and b. These are computed as the ratio of the

standard deviations $a = \frac{\sigma_r}{\sigma_S}$ and respectively as difference of statistical means of the two images $b = a \cdot \mu_r - \mu_s$. This approach, while being simple thus general, was amended by various consecutive improvements [4].

Noting than in our case the content of the two images is very similar, we choose to add more adaptivity by implementing the transfer as:

$$g(u) = \sum_{i=1}^{N} c_i \nu_i(u)(a_i u + b_i) \quad (2)$$

If one chooses $\nu_i(u) = \begin{cases} u, & u \in [u_i^{(m)}, u_i^{(M)}] \\ 0, & otherwise \end{cases}$ and $u_i^{(m)} = u_{i-1}^{(M)} + 1$, then the eq. (2) retrieves the piecewise-consistent color mappings method [10]. Instead of the box-car function with very steep transition used there, we opt for smoother transition typical of fuzzy logic; this aspect will be detailed later in the same section.

Given the histogram of the reference image, $h(I_r)$ and the histogram of the reconstructed image, $h(g(I_s))$ the solution of mapping depicted in eq. (2) can be seen as a minimization problem:

$$minimize_{\mathbf{a},\mathbf{b},\mathbf{c},\nu(u)}(h(I_r) - h(g(I_s))^2 \;\; s.t. \sum_{i=1}^{N} c_i = 1 \quad (3)$$

where $\mathbf{a} = [a_1, \ldots a_N]$, $\mathbf{b} = [b_1, \ldots b_N]$, $\mathbf{c} = [c_1, \ldots c_N]$, $\nu(u) = [\nu_1(u), \ldots \nu_N(u)]$. First, one has to choose a parametric form for the function ν to have the minimization possible. Opting for a boxcar function and solving directly eq. (3), the solution retrieved has $u_i^{(m)} + 1 = u_{i-1}^{(M)}$ and $\mathbf{c}$ as one of the N-dimensional unit vectors; thus it implements the piecewise linear approximation of the eq. (1), that was previously proposed [10]. Modeling with a Gaussian Mixture Model using a maximum posterior probability inference, the mosaicing preprocessing solution [17] is found. Alternatively one may model the histogram as multivariate kernel density and retrieve the mean-shift oriented method [18].

Additional boundary constraints often lead to results that are not necessarily perceptually pleasant. Thus, we consider a different approach inspired from the human perception: the functions ν are taken so to select the color frameworks of the scene, the weights c_i allow even more overlapping between frameworks, while the linear parameters, $\mathbf{a}$, $\mathbf{b}$ are still inspired from the original approach of Reinhard et al. [21].

4.1. Color Frameworks

Although many studies attempted to explain the human perception of complex scenes, no definite model exists. Yet, the reformulation by Gilchrist et al. [6] of the anchoring theory for complex scenes proved to pass many perceptual tests

and explained many phenomena. This anchoring theory focuses on luminance interpretation and states that when depicting a scene, the relation between the representation luminance and the scene lightness can be correctly perceived only through a mapping between the luminance value and the value on the scale of perceived level, process called *anchoring*.

For increasingly complex scenes, the anchoring theory avow that scenes are perceived by the humans in terms of consistent areas, named *frameworks*. A framework is defined as a region of common illumination. For image perception, the human brain estimates the lightness within each framework through the anchoring to the luminance perceived as white, followed by the computation of the global lightness. While the framework theory was developed for luminance images, we assume the same strategy for color images. Intuitively color quantization assumes image organization in frameworks and the perception of quantized scene is appropriate. We consider that scene decomposition in frameworks and performing the transfer between matching frameworks to solve eq. (3) could lead to an interesting color transfer method.

The first computational model of the anchoring theory for complex images was provided by Krawczyk et al. [12] for rendering high dynamic images. This paper follow the same guidelines, with the major difference that for extraction of frameworks instead of the mean-shift, we rely on a thresholded version of Fuzzy C-Means as they allow some image data to be in more than one framework.

We recall that for Fuzzy C-Means (FCM) [3], [1], the following objective function has to be minimized:

$$J_{FCM} = \sum_{k=1}^{P} \sum_{i=1}^{N} \nu_{ik}(x_k - v_i)^2, \;\; s.t. \sum_{i=1}^{N} \nu_{ik} = 1, \forall k \quad (4)$$

where x_k are the 3-dimensional image pixels, P is the total number of pixels, N is the total number of clusters and v_i are the centroids/means of the clusters. The solution (ν_{ik}, v_i) is found iteratively once the number of clusters, N is chosen.

Yet, to increase the functionality of the standard FCM two adaptations are used. First FCM has the known drawback of converging into local optima and simulated annealing was proposed to address this aspect [14]. Convergence into local minima leads to non-overlapping frameworks and visual failure of the transfer. Solving this problem removes this kind of failures. Secondly, even fixed, the FCM, sometimes, converges (truthfully) in unsatisfactory clusters. More precisely cases with large near - saturated areas (in normally exposed image) or near-black ones (in the underexposed image) are separated on different clusters, while the rest of the pixels are in pushed in wide range clusters. Such cases are detected and cluster are merged back.

An illustrative example of the last situation is presented in figure 3.

Intuitively, instead of direct minimization of eq. (2) the optimization is done sequentially, first determining $\nu_i(u) = \nu$ via FCM. In other words, the images are clustered on sets with compact color levels, which may be perceived as a color extension of the frameworks from the anchoring theory.

The two resulting frameworks from the segmented images are similar, but not identical, due to the differences between the initial images, as can be seen in figure 1. Let us denote the frameworks of the reference image by R_i and those of subject image by S_i.

4.2. Implementation

We consider the input images in the CieLab color space as being perceptually consistent. The color transfer implementation follows the procedure:

- *Frameworking*: Determine the frameworks on each of the two images by applying FCM, separately, on both of them. Hard threshold the membership weights, ν so that to select only one framework for each location.

  For each framework, either in subject image, S_i or in the reference image, R_i, compute the mean (μ_i^s and respectively, μ_i^r) and the standard deviations (σ_i^s, σ_i^r).

- *Matching*: Match the frameworks of the low-light image with the ones of the normally exposed. The reference image framework, R_k matching S_i is found as:

$$k = \arg\max_j S_i \cap R_j \qquad (5)$$

  The eq. (5) comes from the fact that the two images contain almost the same scene (i.e. mis-alignment is small), thus we search for maximal spatial overlapping.

- *Framework transfer*: For each pair of frameworks compute a transfer function as in eq. (1). If we denote by $\theta = \{S_i, R_i, \nu_i\}, i = 1 \ldots N$ as the model of the frameworking process, the conditional probabilities $p_{ij}(R_j/\theta)$ of having pixels in the framework R_j that originate in the framework S_i are computed.

  Compute the linear parameters of a subject pixel considered to be in the framework S_i as:

$$a_j = \frac{\sigma_j^r}{\sigma_i^s}; \ \ b_j = \mu_j^r - a_j \cdot \mu_i^s \qquad (6)$$

- *Global transfer*: Compute the image transfer using eq. (2), where the c_i are the framework confusion conditional probabilities: $c_i = p_{ij}(R_j/\theta)$.

We note that while FCM considers tri-dimensional input data, the rest of algorithm is implemented on each color plane separately. At the end the resulting image is converted back to the original color space.

Optimization. To accelerate the process, the FCM runs on low resolution images (e.g. having the width of 640 and the original aspect ratio). On the small resolution image the framework means and variances are found, while the weights are computed on the full resolution image.

5. Results and Discussions

Database. To test the proposed algorithm we collected a specific database using three cameras: a professional one (digital SLR), a consumer one and a smartphone. We have considered two types of differences between the two images forming a set: while the reference image is normally (well) exposed, the low-light images are underexposed with either EV=-1 or EV=-2 (i.e. exposure time is half and respectively a quarter from normal). The images were acquired with hand-held camera, thus they are not perfectly aligned.

In total there have been gathered 100 pairs underexposed with EV=-1 and 100 with EV=-2.

Evaluation. To evaluate the correctness of the color transfer we have acquired, using a tripod a normally exposed image of the photographed scene; this image will be named the evaluation reference image. For evaluation purposes, all corrected images are compared with the evaluation reference image and peak signal–to–noise–ratio (PSNR) and structural similarity - SSIM [26] between the two images are computed. These two measures are typically used to asses the accuracy of reproduction for color transfer methods.

5.1. Results

FCM Resolution. The first encountered problem was due to the time required by the clustering algorithm to run on a high resolution image. In order to make this time acceptable, one may reduce the resolution of the images during clustering, which however lead to another problem: it introduced visible artifacts at the transition between frameworks. For smaller images, the transitions from one framework to others are more noticeable. These transition artifacts appear mainly in the regions that are over–segmented by the FCM algorithm. However computing the pixels weight at full resolution avoided this downside. An example is in figure 2.

Framework merging. The clustering algorithm may produce, at times, an over–segmentation, by artificially splitting near-saturated areas or almost black ones. The proposed solution inspects such frameworks and, at necessity (i.e. framework's means are too close) merges them. An illustrative example is presented in 3 (g), where the lack of merging causes artifacts in the center of the sky in figure.

(a) Ev=0 frameworks   (b) Ev=0   (c) Reconstructed   (d) Ev=-1   (e) Ev=-1 frameworks
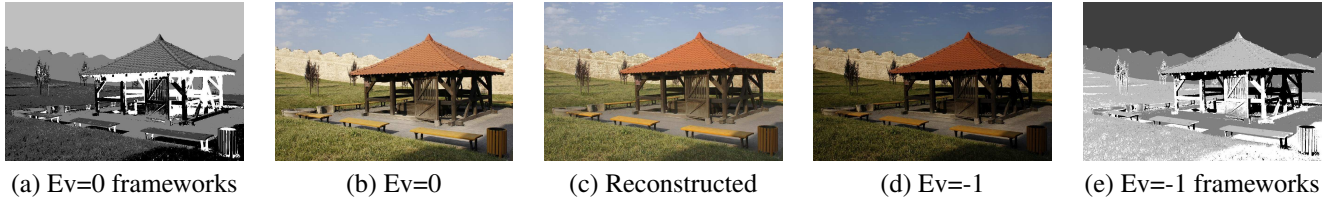
Figure 1. An example showing qualitative result (c). The underexposed image, (d) received the colors from the normally exposed image (b). In (a) are the frameworks of the normally exposed image, while in (e) are the frameworks of the underexposed one.

(a) Ev=0 frameworks   (b) Ev=0   (c) Ev=-1   (d) Ev=-1 frameworks

(e) Ev=-1 corrected frameworks   (f) Final result   (g) Initial result   (h) Detail from (g)
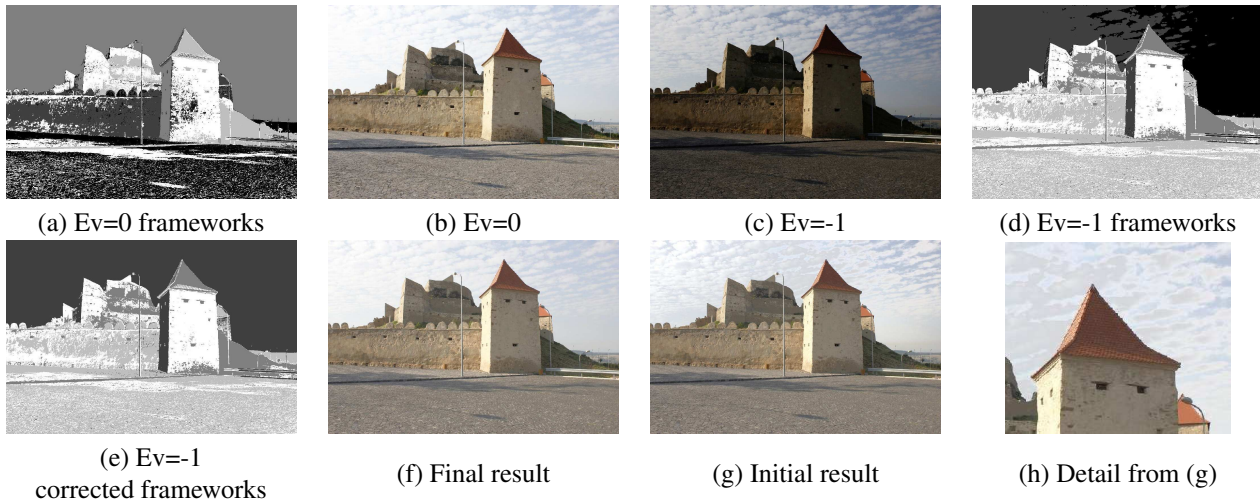
Figure 3. An example that benefits from bad frameworking merging. (b) Original image and (a) its frameworks. (c) Underexposed image and (d) its initial frameworking. Using this frameworking the obtained result is shown in (g). Note the artifacts on the sky, which are detailed in (h). Correcting the over–clustering in the sky, we obtain the frameworking in (e) that produced the final result, shown in (f).

(a)   (b)
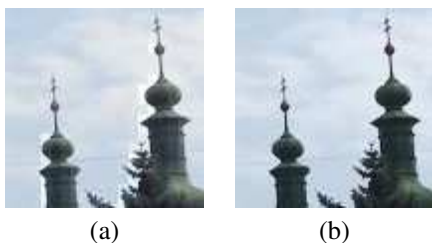
Figure 2. Artifacts at transition may appear if one computes the weights at small resolution (a), compared to computing them at full resolution in figure (b).

Table 1. Achieved performance of the proposed method with respect to camera used.

Camera	EV=-1	EV=-2	All
PSNR			
Smartphone	17.74	17.19	17.47
Consumer	16.93	16.33	16.63
DSLR	17.69	16.85	17.28
SSIM			
Smartphone	0.51	0.50	0.51
Consumer	0.53	0.51	0.52
DSLR	0.54	0.52	0.53

Camera related performance. We report, in table 1, the achieved performance with respect to the camera used. The quality of acquired images is increasing from the smartphone (which has 1.12 μm pixel size), to the consumer camera (with 1.76 μm pixel size) and to the DSLR (with 4.99 μm pixel size). SSIM numerical values indicates that the image quality retrieved using the proposed color transfer method is in accordance with the input image quality.

Comparison with related work. We extensively compare the proposed method with related work [21], [20] and [19] as the authors provide code. The method from [18] has no author provided code, thus we implemented it to our

best ability; this method being based on mean-shift will be denoted by "Mean-Shift".

Numerical results are shown in table 2, while visual, comparative, results are presented in figures 4, 5, 6. We stress that the proposed method is tested on a significantly larger database than related work: in many cases, [19], [10], [18], etc. at most 15 images are used; we test on 200 image sets. Yet, although on particular examples other methods may produce results leading to higher numerical values, overall, and on each category, the proposed method reaches the top performance.

(a) Underexposed Ev=-1   (b) Normal, Ev=0   (c) Proposed

(d) Mean Shift   (e) Pitie et al. [19]   (f) Pouli et al. [20]
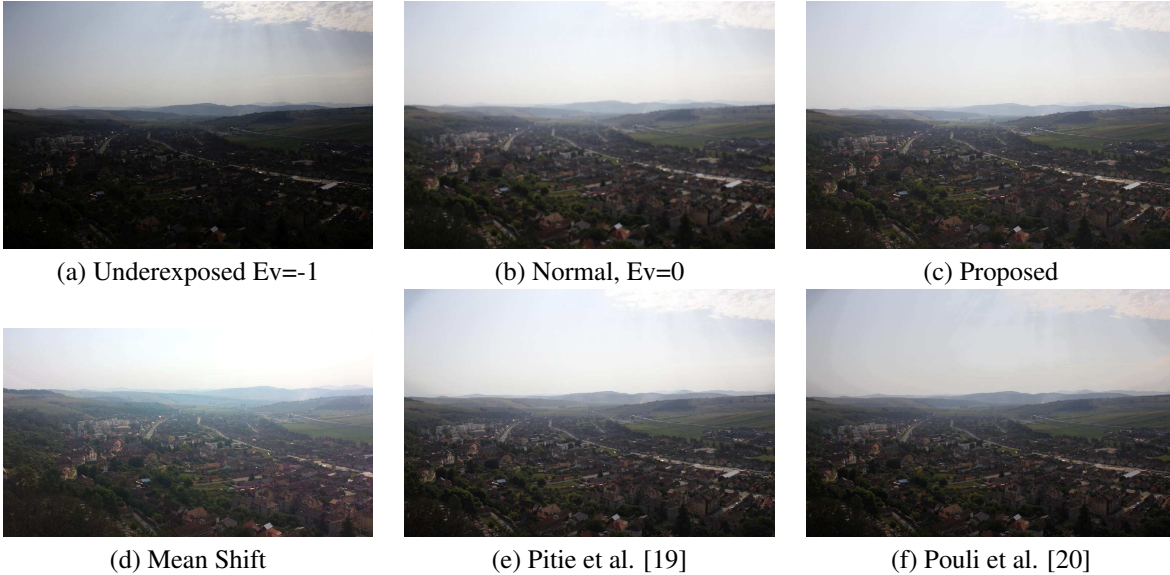
Figure 4. Comparison between proposed method and related work. One may note that the proposed method is closest to the normally exposed image.

Table 2. Numerical comparison between the proposed method and prior related methods.

Method	EV=-1	EV=-2	All
PSNR			
Proposed	17.45	16.48	17.12
Reinhard et al. [21]	16.12	14.75	15.44
Pitie et al. [19]	17.23	16.34	16.79
Pouli et al. [20]	16.66	15.52	16.10
Mean-Shift	16.88	15.97	16.43
SSIM			
Proposed	0.53	0.51	0.52
Reinhard et al. [21]	0.50	0.48	0.49
Pitie et al. [19]	0.52	0.50	0.51
Pouli et al. [20]	0.52	0.49	0.50
Mean-Shift	0.51	0.48	0.49

From a subjective point of view there are further observations to be laid down. Artifacts of the proposed method, while exist, they are rarer and less disturbing than those of other solutions. Typical artifacts are related to incorrect colors and some visible transitions. By contrast, in the initial algorithm [21], there aren't any transition artifacts since the image is considered as a whole. However global transfer leads to poor color in smaller regions, thus explaining the lowest reported results from table 2.

Figure 4 contains an outdoor image where all discussed methods performed reasonably well. Yet the mean-shift solution produced a greenish tint over the sky due to larger weight of foreground. The proposed method and the ones from [19] and [20] produced images consistent with the ref-

erence. However this is no longer the case with the examples from figure 5 where the other methods, [19], [20], produced visible artifacts (fake colors and artificial objects) on the tower and respectively on the sky.

Following the comparison with the mean-shift based algorithm [18] through figures 4, 5, 6, one may note that the results for the later are inconsistent. The main problem of the mean-shift is that using the same parameter for the Parzen window bandwidth, while on some images good results are achieved (as in figures 4-(d), 5-(d)), on others, disturbing artifacts are obtained (5-(h))). Also on some cases the resulting clusters are too large leading to insufficient contrast (as in figure 6 (c) and (h)).

Comparison with blind deconvolution. In figure 7 the proposed approach is demonstrated on a case where the normally exposed image is visibly blurred. To minimize the time-lap between he two images, the normally exposes is was acquired to be smaller and with distorted aspect ratio. For deconvolution we have the blind patch recurrence solution [16]. Blind deconvolution introduces visible artifacts by reducing the actual resolution.

6. Conclusions

In this paper we argue that, while facing potential motion blur is more efficient to underexpose images and perform color transfer for low-light compensation than implement blur deconvolution. Furthermore, we have introduced a generative model for color transfer and we show that many previously introduced methods may be retrieved as particular cases of it. At last we have introduced a color transfer method that is shown to outperform related methods on a

(a) Normal, Ev=0	(b) Underexposed Ev=-1	(c) Proposed
(d) Mean-Shift	(e) Pitie et al. [19]	(f) Pouli et al. [20]
(e) Normal, Ev=0	(f) Underexposed Ev=-1	(g) Proposed
(h) Mean-Shift	(i) Pitie et al. [19]	(j) Pouli et al. [20]
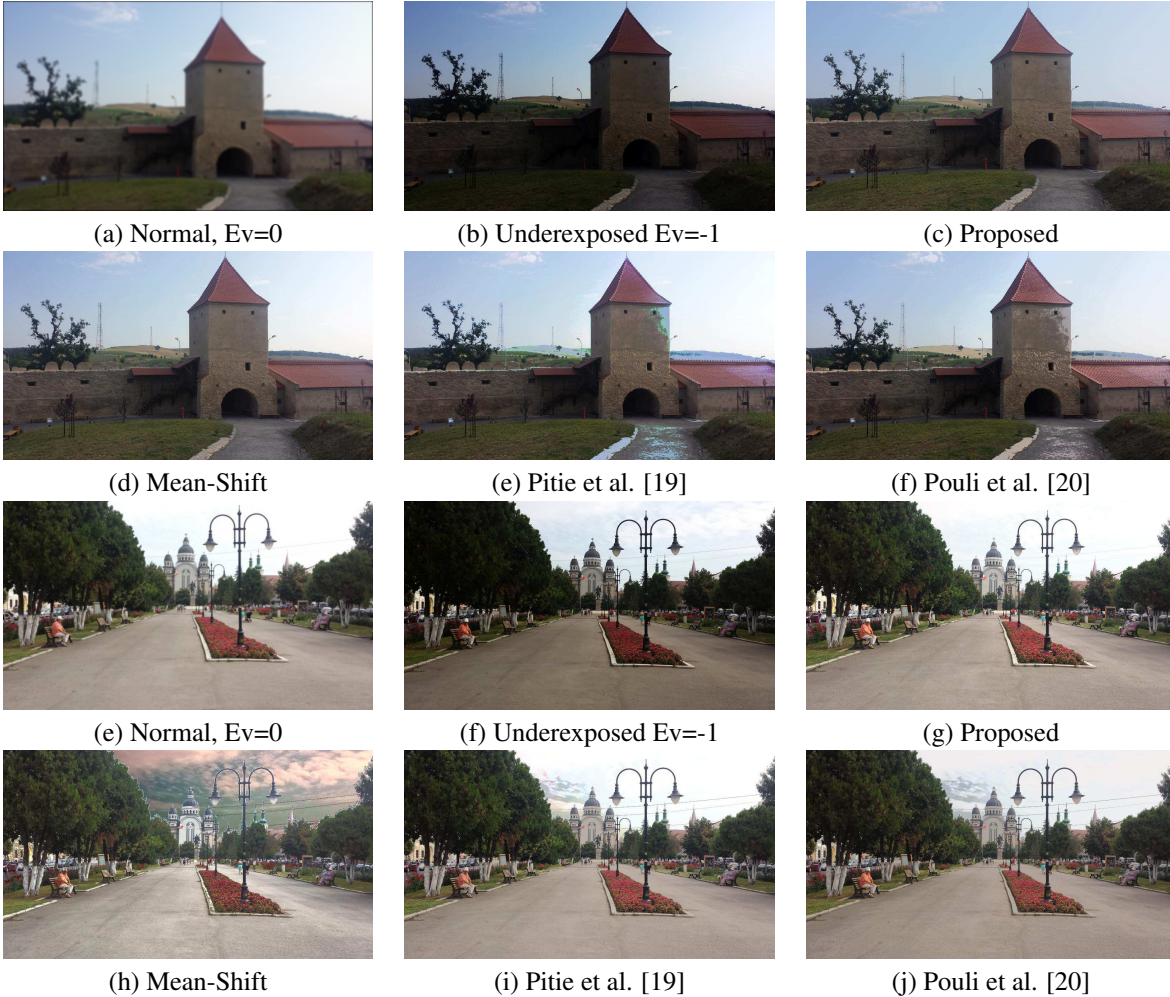
Figure 5. Comparison between proposed method and related work. One may note the mis-alignment between acquired images and the fact the normally exposed image is slightly blurred.

substantially large image database.

Subjective evaluations show that images without visible quality degradation are computed while underexposing with 2 EV stops (i.e. taking a quarter from the exposure time required by the scene nominal illumination). The algorithm is subject to full optimization and may be implemented inside a camera.

References

[1] J. C. Bezdek. *Pattern Recognition with Fuzzy Objective Function Algoritms*. Plenum Press, New York, 1981.

[2] A. Drimbarean, A. Zamfir, F. Albu, V. Poenaru, C. Florea, P. Bigioi, E. Steinberg, and P. Corcoran. Low-light video frame enhancement, 2007. US Patent 8199222.

[3] J. C. Dunn. A fuzzy relative of the isodata process and its use in detecting compact well-separated clusters. *Journal of Cybernetics*, 3:32–57, 1973.

[4] H. S. Faridul, T. Pouli, C. Chamaret, J. Stauder, A. Tremeau, and E. Reinhard. A Survey of Color Mapping and its Applications. In S. Lefebvre and M. Spagnuolo, editors, *Eurographics 2014 - State of the Art Reports*. The Eurographics Association, 2014.

[5] K. Fotiadou, G. Tsagkatakis, and P. Tsakalides. Low light image enhancement via sparse representations. In *Proc. of Int. Conf. on Image Analysis and Recognition*, volume 8814, pages 84–93. LNCS, 2013.

[6] A. Gilchrist, C. Kossyfidis, F. Bonato, T. Agostini, J. Cataliotti, X. Li, B. Spehar, V. Annan, and E. Economou. An anchoring theory of lightness perception. *Psychological Review*, 106(4):795–834, 1999.

(a) Underexposed, Ev=-1 (b) Proposed (c) Mean Shift

(d)) Pitie et al. [19] (e) Pouli et al. [20]

(f) Underexposed, Ev=-2 (g) Proposed (h) Mean Shift

(i) Pitie et al. [19] (j) Pouli et al. [20]
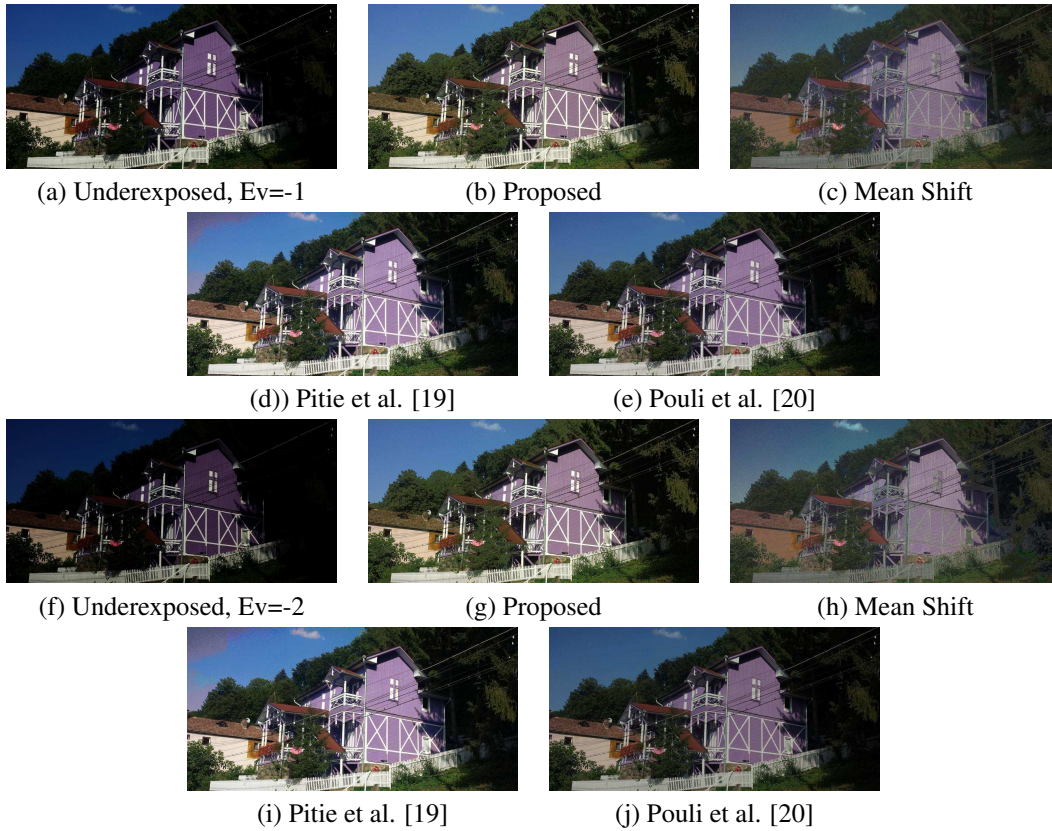
Figure 6. Comparison between proposed method and related work. The same scene underexposed with one EV stop (top two rows, (a) - e)) and respectively with two stops (bottom two rows, (f) - (j)). Note the artifacts produced by other solutions on the house and on the sky.

(a) Underexposed Ev=-1 (b) Normal, Ev=0

(c) Proposed (d) Blind deblurred [16]
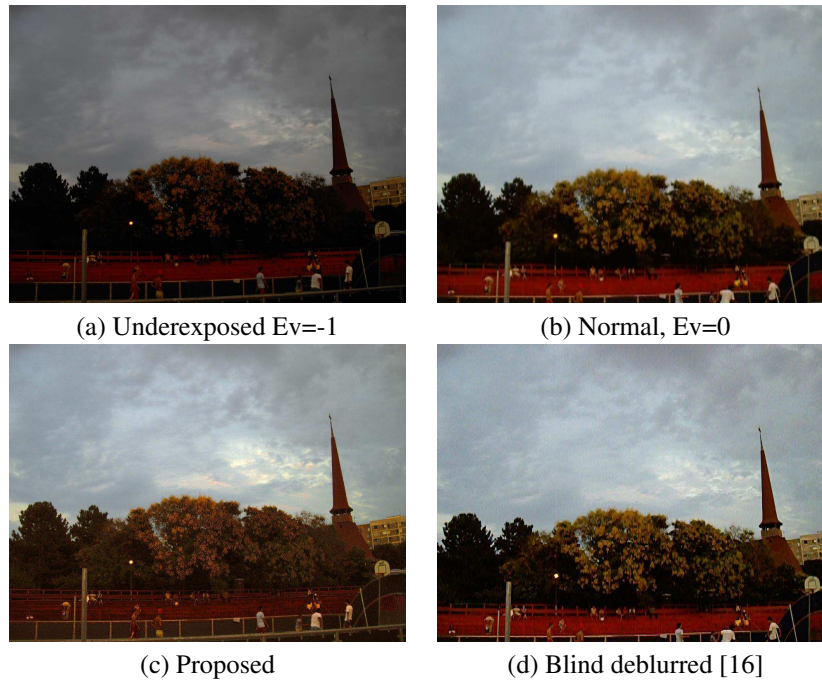
Figure 7. Comparison between proposed method and a blind deconvolution method [16]. One may note that the deconvolution introduces noticeable artifacts.

[7] A. Gupta, N. Joshi, L. Zitnick, M. Cohen, and B. Curless. Single image deblurring using motion density functions. In *Proc. ECCV*, pages 171–184, 2010.

[8] M. Hirsch, C. J. Schuler, S. Harmeling, and B. Scholkopf. Fast removal of non-uniform camera shake. In *Proc. of ICCV*, pages 463–470, 2011.

[9] N. Joshi, S. B. Kang, C. Lawrence-Zitnick, and R. Szeliski. Image deblurring using inertial measurement sensors. *ACM TOG*, 29(4):30, 2010.

[10] S. Kagarlitsky, Y. Moses, and Y. Hel-Or. Piecewise-consistent color mappings of images acquired under various conditions. In *Proc. ICCV*, pages 2311–2318, 2009.

[11] J. Kotera and F.Sroubek. Review of recent developments in image blind deconvolution. In *Proc. WDS*, volume 1, pages 76–81, 2012.

[12] G. Krawczyk, K. Myszkowski, and H.-P. Seidel. Lightness perception in tone reproduction for high dynamic range images. In *Proc. of Eurographics, Computer Graphics Forum*, volume 24, 2005.

[13] A. Levin, Y. Weiss, F. Durand, and W. Freeman. Understanding blind deconvolution algorithms. *IEEE T. PAMI*, 33(12):2354–2367, 2011.

[14] P. Liu, L. Duan, X. Chi, and Z. Zhu. An improved fuzzy c-means clustering algorithm based on simulated annealing. In *Proc. FSKD*, pages 39–43, 2013.

[15] K. G. Lore, A. Akintayo, and S. Sarkar. Llnet: A deep autoencoder approach to natural low-light image enhancement. *CoRR*, abs/1511.03995, 2015.

[16] T. Michaeli and M. Irani. Blind deblurring using internal patch recurrence. In *Proc of ECCV*, pages 783–798, 2014.

[17] M. Oliveira, A. D. Sappa, and V. Santos. Unsupervised local color correction for coarsely registered images. In *Proc. CVPR*, pages 201 – 208, 2011.

[18] M. Oliveira, A. D. Sappa, and V. Santos. A probabilistic approach for color correction in image mosaicking applications. *IEEE TIP*, 24(2):508–523, 2015.

[19] F. Pitie, A. Kokaram, and R. Dahyot. Automated colour grading using colour distribution transfer. *CVIU*, 107:123–137, 2007.

[20] T. Pouli and E. Reinhard. Progressive color transfer for images of arbitrary dynamic range. *Computers & Graphics*, 35(4):67–80, 2011.

[21] E. Reinhard, M. Ashikhmin, B. Gooch, and P. Shirley. Color transfer between images. *IEEE Computer Graphics and Applications*, 21(5):34–41, 2001.

[22] D. Ruderman, T. Cronin, and C. Chiao. Statistics of cone responses to natural images: Implications for visual coding. *JOSA A*, 15(8):2036–2045, 1998.

[23] S. P. N. Singhy and C. N. Riviere. Physiological tremor amplitude during retinal microsurgery. In *Proc. of the IEEE Bioengineering Conf.*, pages 171–172, 2002.

[24] J. Sun, W. Cao, Z. Xu, and J. Ponce. Learning a convolutional neural network for non-uniform motion blur removal. In *Proc. CVPR*, pages 769 – 777, 2015.

[25] K. Veluvolu and W. T. Ang. Estimation and filtering of physiological tremor for real-time compensation in surgical robotics applications. *Int J Med Robotics Comput Assist Surg*, 6:334–342, 2010.

[26] Z. Wang, A. C. Bovik, H. R. Sheikh, and E. P. Simoncelli. Image quality assessment: from error visibility to structural similarity. *IEEE TIP*, 13(4):600–612, 2004.

[27] O. Whyte, J. Sivic, A. Zisserman, and J. Ponce. Non-uniform deblurring for shaken images. *IJCV*, 98(2):168–186, 2012.

[28] F. Xiao, J. Pincenti, and J.Farrell. Camera motion and effective spatial resolution. In *Proc. Int. Congress of Imaging Science*, volume I, pages 33 – 36, 2006.

[29] L. Yuan, J. Sun, L. Quan, and H. Shum. Blurred/non-blurred image alignment using sparseness prior. In *Proc. ICCV*, pages 1 – 8, 2007.